J. Astrophys. Astr. (2016) 37: 3

Development of a Code to Analyze the Solar White-Light Images from the Kodaikanal Observatory: Detection of Sunspots, Computation of Heliographic Coordinates and Area

Ragadeepika Pucha[1], K. M. Hiremath[2] & Shashanka R. Gurumath[3,*]
[1]*Integrated Science Education and Research Center (ISERC), Visva-Bharati University, Santiniketan 731 235, India*
[2]*Indian Institute of Astrophysics, Bangalore 560 034, India*
[3]*VIT University, Vellore 632 014, India*
[*]*e-mail: shashankgurumath@yahoo.in*

Received 23 July 2015; accepted 19 November 2015
DOI: 10.1007/s12036-016-9370-4

Abstract. Sunspots are the most conspicuous aspects of the Sun. They have a lower temperature, as compared to the surrounding photosphere; hence, sunspots appear as dark regions on a brighter background. Sunspots cyclically appear and disappear with a 11-year periodicity and are associated with a strong magnetic field ($\sim 10^3$ G) structure. Sunspots consist of a dark umbra, surrounded by a lighter penumbra. Study of umbra–penumbra area ratio can be used to give a rough idea as to how the convective energy of the Sun is transported from the interior, as the sunspot's thermal structure is related to this convective medium.

An algorithm to extract sunspots from the white-light solar images obtained from the Kodaikanal Observatory is proposed. This algorithm computes the radius and center of the solar disk uniquely and removes the limb darkening from the image. It also separates the umbra and computes the position as well as the area of the sunspots. The estimated results are compared with the Debrecen photoheliographic results. It is shown that both area and position measurements are in quite good agreement.

Key words. Sun—sunspots—Kodaikanal digitized data—sunspot area —heliographic coordinates.

1. Introduction

Sunspots are the visible indicators of magnetic activity on the Sun. These activities are associated with the highly energetic particles that are spewed into space, which in turn affect the Earth's climate and environment (Hiremath & Mandi 2004; Hiremath 2006a, b, 2009; Hiremath *et al.* 2015). Proper estimation of position and area of sunspots is crucial for understanding many solar phenomena, such as rotation rate of the Sun, the solar irradiance that changes from one cycle to another, etc.

Accurate computation of the position of sunspots helps in accurately estimating the meridional flows whose cyclic dependency is supposed to dictate the amplitudes of the solar cycle. The other studies involving sunspots include growth and decay of spots (Lustig & Wohl 1995; Hiremath & Lovely 2010), emergence of flux due to spots (Baranyi & Ludmany 1992), evolution of sunspot groups and interaction between them (van Driel-Gesztelyi *et al.* 1993), axial tilt of sunspot groups (Howard 1991, 1992) and periodicities in solar activity (Oliver & Ballester 1995).

Initially attempts for sunspot detection from the solar images included threshold intensities for umbra–penumbra and penumbra–photosphere boundaries (Grossmann-Doerth & Schmidt 1981; Steinegger *et al.* 1990). To derive the threshold, cumulative histogram methods were adopted (Pettauer & Brandt 1997). Another method (Pettauer & Brandt 1997) to detect the sunspots included the maximum gradient method. Some others (Chapman & Walton 2001) applied edge-detection method to extract objects from background. Gyori (1998) and Zharkov *et al.* (2005) adopted morphological operations in addition to gradient measures to detect the edge of sunspots. Curto *et al.* (2008) and Watson *et al.* (2009) used morphological tools to detect the sunspots. A new method based on the level-set formulation of active contour was proposed by Goel & Mathew (2014). Adaptive region growing techniques are yet another method (Yu *et al.* 2014) for detection of sunspots.

Many methods to compute the position and area of sunspots were used (Howard *et al.* 1984; Baranyi *et al.* 1999; Cakmak 2014). The Greenwich photoheliographic results (GPR) compiled sunspot observations from a small network of observatories to produce a catalog of sunspots from 1874 to 1976. By overlapping Stonyhurst charts (with spherical grids) manually, average position between two grids in which the sunspot is inscribed within a square box is estimated. In Debracen photoheliographic data, the position of a spot is derived from the position of the center of the umbra (Csilla Szasz 2003, if the umbra could be separated from the penumbra. If there is no identification of any umbra in the penumbra, the position of the center of the penumbra is measured. Some other such methods have been described in Poljancic *et al.* (2011).

We have a treasure of more than 100 years white-light and calcium picture data from the Kodaikanal Observatory, which is digitized recently (Singh & Ravindra 2012; Ravindra *et al.* 2013). In the present study, we analyze only the white-light images. These images were previously analyzed by using the reduction techniques used for calculation of Mt.Wilson measurements (Howard *et al.* 1984; Sivaraman & Gupta 1993). In this method, a cross-hair is positioned over the umbra and the position is computed to be the mean position of vertices of the cross-hair. The areas were determined to be that of the superimposed quadrilateral by the cross-hair. For the same data set, Ravindra *et al.* (2013) proposed another method involving morphology for sunspot area measurement, although limb darkening was not removed and the heliographic coordinates were not computed. In order to complete the task, in this study an algorithm is proposed to locate the center and radius of the solar disk and to remove limb darkening from the image. This algorithm further detects the sunspots, separates the umbra from it and calculates the position (heliographic coordinates) and area of sunspots with proper error bars. Section 2 outlines the details of observation of the images from the Kodaikanal Observatory. Section 3 describes the method of analysis in detail and finally, section 4 presents the comparison of the estimated results with those of the Debracen results.

2. Observational details

The solar telescope at the Kodaikanal Observatory consists of a 15-cm achromatic lens as the objective, which has a focal length of 240 cm. In the focal plane a green color filter is used to improve the quality of the solar image. More detailed information of this telescope can be found in Sivaraman & Gupta (1993).

Photographic data of the Sun extends back to 1904 and is available up to present day. The telescope produces a solar disk image which is about 20 cm in diameter. Most of the images are taken early in the morning, before 10 h (IST). On most days, only one image is obtained and some days, few more images are obtained, depending on the sky conditions. A typical white light image of the Sun obtained from the Kodaikanal Observatory is illustrated in Figure 1. One can notice a straight line (thin wire), that marks the east–west direction of the sky on the image.

The solar white-light images were stored on the photographic plates of size 25.4 sq. cm till 1975. From Jan. 1976, they were replaced by high-contrast film of size 25.4 cm $\times$ 30.5 cm. These photographic plates were carefully preserved along with a log book about the information of the observations. In almost 106 years of observations, 31800 plates covering over 31000 days are available. All these photographic images were digitized recently using a proper 4k $\times$ 4k format CCD-camera. The whole process of this digitization and calibration of the images is described by Ravindra *et al.* (2013).

3. Data analysis

Sunspot detection is a tricky procedure. Computation of accurate heliographic coordinates is another difficult task without which no meaningful science can be derived from the solar images. For this purpose, the following procedures have to be adopted. First and foremost is to detect the edge of the solar disk. Then one has to compute its center and radius uniquely, remove the limb darkening from the image and then

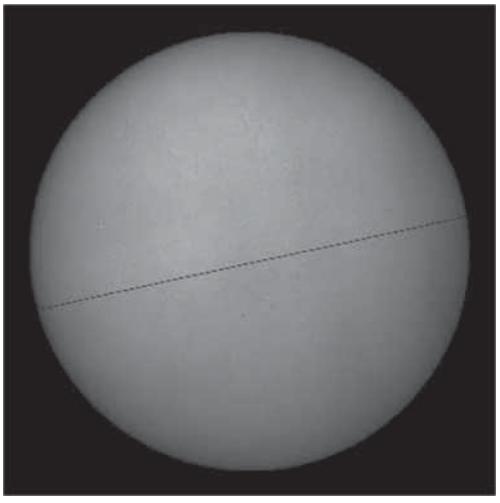

Figure 1. Digitized white-light image of the Sun obtained from Kodaikanal Solar Observatory.

the heliographic coordinates of each pixel of the image are to be obtained. Further, the sunspots are detected, the umbra is separated and the average heliographic coordinates and the area of the sunspots are calculated. Each of these steps are briefly explained in the following sub-sections.

3.1 *Detection of the edge*

In order to estimate the heliographic coordinates, it is important to calculate the center and radius of the solar disk. This requires detection of edge of the image as accurately as possible. A sobel operator is used for the edge detection for each of the images. This filter uses the concept of sudden gradient change at the edges. A typical solar white-light image with its detected edge is illustrated in Figure 2.

3.2 *Calculation of center and radius*

The next major step is the computation of the center and radius of the solar disk in terms of number of pixels. These parameters are quite crucial for the positional measurements on the Sun. Many different methods were adopted in the past (Denker *et al.* 1998). For Kodaikanal images, Hough transform was used to locate the solar disk center and radius (Ravindra *et al.* 2013). According to them, with the radius of the Sun as a free parameter, eight points on the edge are considered and the circle is fitted for obtaining the central coordinates of the disk. With this method, there is a possibility that the coordinates of the disk center are estimated wrongly if the given radius is incorrect. Hence, in order to compute uniquely all the three parameters (two coordinates of the center and radius) as described in Appendix A, the method of circle-fitting is used. In our method, all the detected points of the edge are used for fitting the circle. A least-square fitting is applied to find the best fit. This involves solving for three unknowns (two center coordinates and one radius) with three

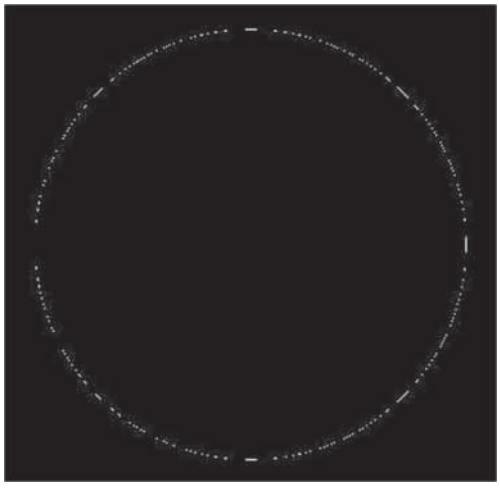

Figure 2. Detected edge (white dots) of the solar disk from Kodaikanal Solar Observatory.

equations. Hence, all the three parameters are obtained simultaneously and uniquely. This procedure is applied for each of the images to locate the disk center and radius.

3.3 *Removal of limb darkening*

While observing the Sun, there is a gradual decrease in intensity from center of the disk to the limb. This apparent change in intensity is called as limb darkening (see Figure 3). It is very crucial to remove this effect before any further analysis of the Sun's images. To remove limb darkening, the following procedure is adopted on each of the images.

For each of the images, concentric circles are drawn from the center to the edge, each of whose radius increases by one unit. The median of intensities in each of the

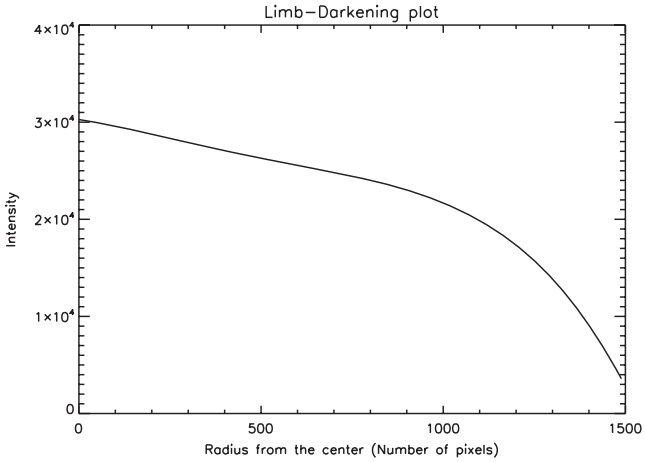

Figure 3. Variation of median intensity from disk center to the edge of the solar disk.

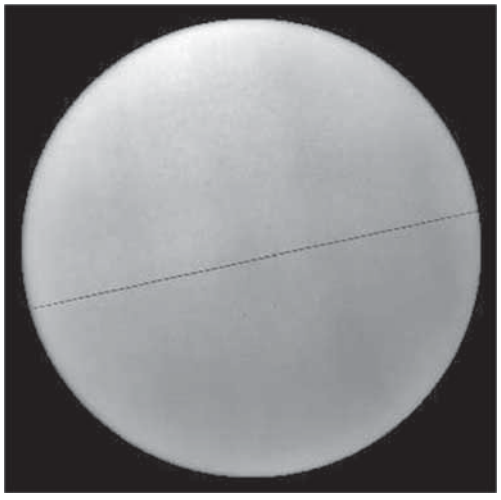

Figure 4. Solar white light image after limb darkening removal.

concentric circles corresponding to that radius are estimated. Hence, a fixed intensity for each radius value is obtained. A polynomial of degree 3 fits very well for these radius-intensity values (Figure 3). If r is the radius of a particular pixel, I is its intensity and $I(r)$ is its intensity profile according to the fit, then its corrected value is

$$I_{\text{corrected}} = \frac{I}{I(r)}.$$

This intensity correction is applied for all the pixels in each of the digitized images, resulting in uniformly bright images, hence suggesting that the phenomenon of limb darkening has been removed from the images. One such processed image is illustrated in Figure 4.

3.4 *Detection of sunspot and separation of umbra*

The main techniques used for the detection of sunspots from the Kodaikanal solar images are from the field of mathematical morphology. Several studies earlier used this method to detect sunspots (Zharkov *et al.* 2005; Curto *et al.* 2008). This method uses shape and structure of digital images to analyze the features present in the image. It uses a certain structuring element to probe the image, which maybe of any shape but, a circle, square or cross are commonly used. The basic operations of morphology include erosion, dilation, opening, closing and top-hat transformation.

After the limb darkening is removed, the image is inverted by taking the reciprocal of intensities at each point. This transformation results in the sunspots appearing brighter on a darker background. Histogram equalization is then applied to this image, that adjusts the image intensities to enhance the contrast (Figure 5). This makes it easier to extract sunspots from the image. Next, a top-hat transformation is applied. The structuring element used in this case is a disk of radius 50 units. A certain intensity threshold that is derived by taking mean of values from several

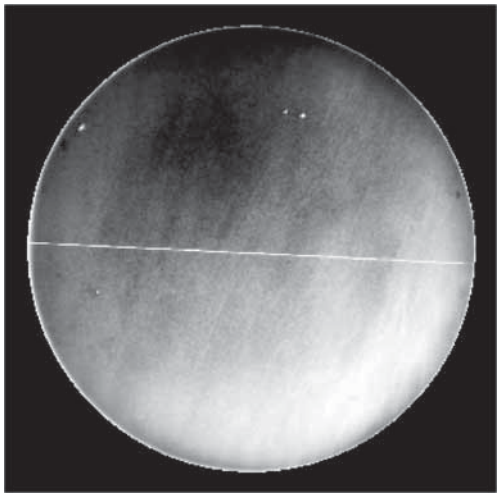

Figure 5. The image that is inverted by taking the reciprocal of intensities at each point is illustrated.

sunspots is applied. As a result, a frame consisting of only the bright sunspot regions is obtained. After applying mask filter over these regions that makes the intensity of all the selected regions equal to unity, they are multiplied with the original image to obtain only the sunspot regions in the image.

After the sunspot regions are detected, each region is normalized by dividing the intensities of sunspot's pixels with its maximum value. An intensity threshold that is unique for each of these regions is then applied. The threshold is 15% more than the minimum value in each region. This threshold is taken by observing several sunspots and considering the mean intensity of all the values. These processes are repeated for each of the images to obtain the umbra separated from all the sunspots.

An example of the extracted sunspot and its umbra is given in Figure 6.

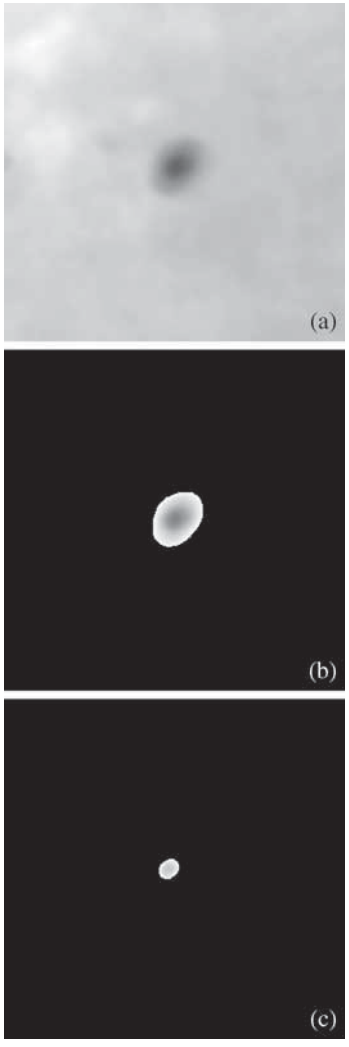

Figure 6. An example of the detection. (**a**) Typical sunspot, (**b**) extracted sunspot and (**c**) separated umbra.

3.5 *Computation of heliographic coordinates of sunspots*

Before the heliographic coordinates of the sunspots are computed, heliographic coordinates of each pixel of the solar disk of each image is computed. Detailed steps of computation of these heliographic coordinates are presented in Appendix B. After this computation, sunspots are detected as described in the previous section. Then, the average heliographic latitude, θ_{spot} and average heliographic longitude difference, l_{spot}, with their error bars ($\delta\theta$ and δl) are computed as follows.

If θ_n, l_n and I_n are latitude, longitude difference and intensity of the n-th pixel of the detected sunspot, then following Hiremath and Hegde (2013), the average heliographic coordinates of the sunspot are the weighted means as given below:

$$\theta_{\text{spot}} = \frac{\sum_n \theta_n \times I_n}{\sum_n I_n}$$

and

$$l_{\text{spot}} = \frac{\sum_n l_n \times I_n}{\sum_n I_n}.$$

The errors, $\delta\theta$ and δl in these heliographic coordinates are computed as follows.

$$\delta\theta = \frac{\sigma_\theta}{\sqrt{N}}$$

and

$$\delta l = \frac{\sigma_l}{\sqrt{N}}.$$

Here, σ_θ and σ_l denote standard deviation of latitude and longitude difference values of the sunspot pixels, and N is the total number of pixels in the considered spot. Using the above mentioned formulae, the heliographic coordinates and their errors for each sunspot in every image are estimated.

3.6 *Computation of area of sunspot*

The area of the whole spot and that of the umbra are calculated separately. In general, area is the product of number of pixels and area of each pixel. If one knows the size of a pixel, then area of pixel is square of the pixel size. Pixel size is computed as follows:

$$\text{Pixel size} = \frac{\text{Radius of sun in arcseconds}}{\text{Radius of sun in pixels}} = \frac{\text{Rad}}{R}$$

where the computations of Rad and R are given in Appendix B.

The number of pixels in the whole spot and umbra is then estimated and multiplied by the area of the pixel. This area is then expressed in millionth of area of solar hemisphere, which is the standard unit for measuring the area of sunspots.

The Sun is a sphere, but it is flattened on the image. This leads to some projection effects at the edge of the Sun. Owing to the spherical shape of the Sun, the area of sunspots appear less than the true area. This effect is also called as the foreshortening of the area. This projection effect is corrected as follows:

$$\text{Area, } A' \text{ of sunspot } = \text{ No. of pixels } \times \text{ pixel area,}$$

$$\text{Corrected Area } (A) \ = \ \frac{A'}{\cos(\delta)},$$

where $\cos(\delta) = \sin(B_o)\sin(\theta) + \cos(B_o)\cos(\theta)\cos(l)$, with θ and l are heliographic latitude and heliographic longitude from the central meridian of the sunspot respectively, whereas B_o is the heliographic latitude of the center of the solar disk at the time of observation.

Errors in the area of the whole sunspot and umbra are determined by moving the boundary inwards and outwards by one pixel, since we are confident in locating the boundaries to within one pixel of their true location. The penumbra area is then calculated by subtracting the umbra area from the whole spot area and the required umbra–penumbra area ratio is then obtained.

Table 1. Estimated center and radius values.

Year	Month	Date and Time	X-center	Y-center	Radius (No. of pixels)
2011	1	1.340278	2048	2048	1522.84
2011	1	2.362500	2048	2048	1519.16
2011	1	4.340278	2048	2048	1523.65
2011	1	5.315972	2048	2048	1523.06
2011	1	5.345139	2048	2048	1526.33
2011	1	6.331250	2048	2048	1521.75
2011	1	7.322917	2048	2048	1522.77
2011	1	8.347222	2048	2048	1524.53
2011	1	9.383333	2048	2048	1524.16
2011	1	10.427083	2048	2048	1523.38
2011	1	11.333333	2048	2048	1525.38
2011	1	12.438889	2048	2048	1526.99
2011	1	13.395833	2048	2048	1524.86
2011	1	16.625000	2048	2048	1523.68
2011	1	17.333334	2048	2048	1523.06
2011	1	18.322916	2048	2048	1522.81
2011	1	18.447916	2048	2048	1523.94
2011	1	19.329861	2048	2048	1522.96
2011	1	20.336805	2048	2048	1522.85
2011	1	21.340279	2048	2048	1523.38
2011	1	22.324306	2048	2048	1521.30
2011	1	23.326389	2048	2048	1522.54
2011	1	24.326389	2048	2048	1519.10
2011	1	25.364584	2048	2048	1521.62
2011	1	26.322916	2048	2048	1521.07
2011	1	27.597221	2048	2048	1521.92
2011	1	28.345139	2048	2048	1522.67
2011	1	29.378471	2048	2048	1522.31
2011	1	30.338194	2048	2048	1520.16
2011	1	31.340973	2048	2048	1519.98

Table 2. Estimated heliographic coordinates, whole spot area and umbra–penumbra area ratio of sunspots.

Year	Month	Date and Time	θ	$\delta\theta$	l	δl	WA	δWA	UA	δUA	PA	δPA	$\frac{UA}{PA}$	$\delta\frac{UA}{PA}$
2011	2	2.440972	−23.081	0.011	−13.103	0.012	30.338	5.641	15.509	3.480	14.829	2.160	1.046	0.082
2011	2	2.440972	−20.409	0.012	−6.092	0.010	24.599	4.690	12.006	3.075	12.593	1.615	0.953	0.122
2011	2	3.326389	−20.252	0.011	6.213	0.011	15.201	3.450	8.078	2.497	7.123	0.953	1.134	0.199
2011	2	4.649305	−18.673	0.010	−6.566	0.012	30.020	5.032	9.546	2.769	20.474	2.263	0.466	0.084
2011	2	4.649305	−17.985	0.013	−4.470	0.010	34.042	5.432	17.096	3.839	16.946	1.592	1.009	0.132
2011	2	8.324306	15.616	0.012	57.380	0.021	35.037	10.026	0.000	0.000	35.037	10.026	0.000	0.000
2011	2	9.357639	19.947	0.011	−33.471	0.015	19.413	5.661	12.526	3.538	6.886	2.123	1.819	−0.047
2011	2	10.331250	−20.734	0.009	−24.280	0.017	26.736	5.382	7.594	2.558	19.142	2.824	0.397	0.075
2011	2	10.331250	−20.591	0.008	−18.231	0.020	31.826	6.904	9.593	3.989	22.233	2.915	0.431	0.123
2011	2	11.333333	−20.234	0.011	−3.805	0.014	42.368	6.543	10.567	4.009	31.801	2.534	0.332	0.100
2011	2	12.329861	−19.651	0.011	−21.519	0.012	40.469	6.013	9.435	2.729	31.033	3.283	0.304	0.056
2011	2	12.329861	−19.399	0.011	−26.641	0.012	34.884	5.492	9.066	2.833	25.818	2.659	0.351	0.074
2011	2	12.329861	19.272	0.015	−26.321	0.010	25.199	6.800	8.407	3.009	16.792	3.791	0.501	0.066

4. Results

In order to compute heliographic coordinates and area of sunspots, white-light images for the year 2011 of the Kodaikanal Observatory are considered. As described in section 3, edge of solar disk is detected, the effect of limb darkening is removed, radius and center coordinates are simultaneously and uniquely estimated; then sunspots are detected, umbra–penumbra are separated and finally the respective heliographic coordinates and areas are estimated. After the complete analysis, two files – one containing the radius values for each day and another containing the latitude, longitude and umbra area to penumbra area ratio for each sunspot – are obtained. A typical table of center and radius values daily for the images of January, 2011 is given in Table 1. In Table 2, a part of the final result file for February 2011 is given. For each detected sunspot, the date and time of observation, the heliographic coordinates (θ and l) with the respective error bars ($\delta\theta$ and δl), the corrected whole spot

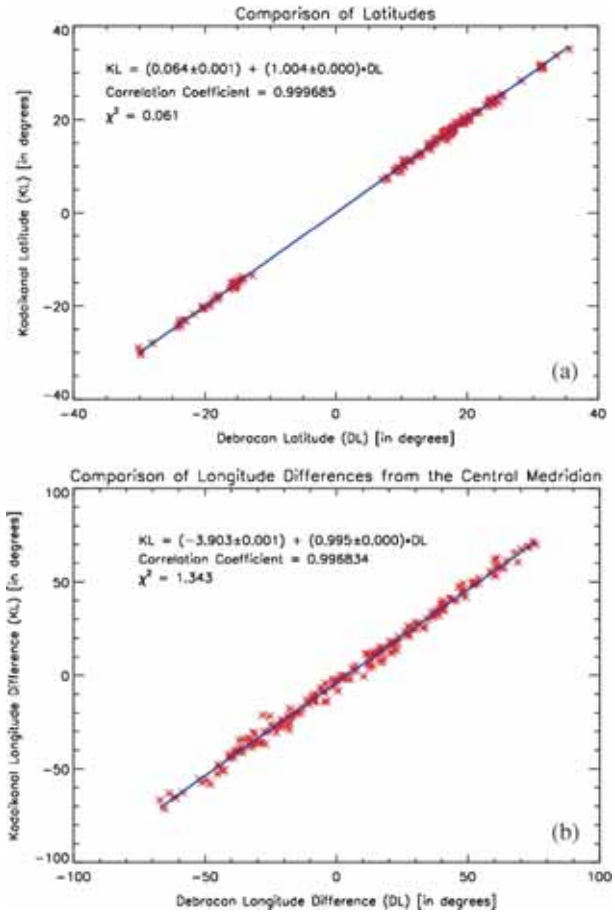

Figure 7. A scatter plot of Kodaikanal and Debracen sunspot data for heliographic coordinates. (**a**) The scatter plot for latitudes, and (**b**) the scatter plot for longitudes from the central meridian.

area (WA), the umbra area (UA), the penumbra area (PA) and the umbra–penumbra area ratio (UA/PA) with the corresponding error bars are presented.

In order to validate our detected method of sunspots and computation of their area and heliographic coordinates, the different parameters of the sunspots are compared with the estimated parameters obtained from different studies. One such comparison with the results of Debracen sunspot data is presented in this study. Typical scatter plots of heliographic coordinates (Figures 7), area (Figures 8) and umbra–penumbra area ratio (Figures 9) are presented. Monthly average variation of whole spot area and umbra–penumbra area ratio (Figures 10) for a period of one year is also plotted and compared with the Debracen data.

From all these results, one can notice from the scatter plots that there is almost a perfect association between Kodaikanal and Debracen results, hence validating our method of detection of sunspots and the estimation of their heliographic coordinates and area respectively. In fact, the goodness of fit and association is judged by the

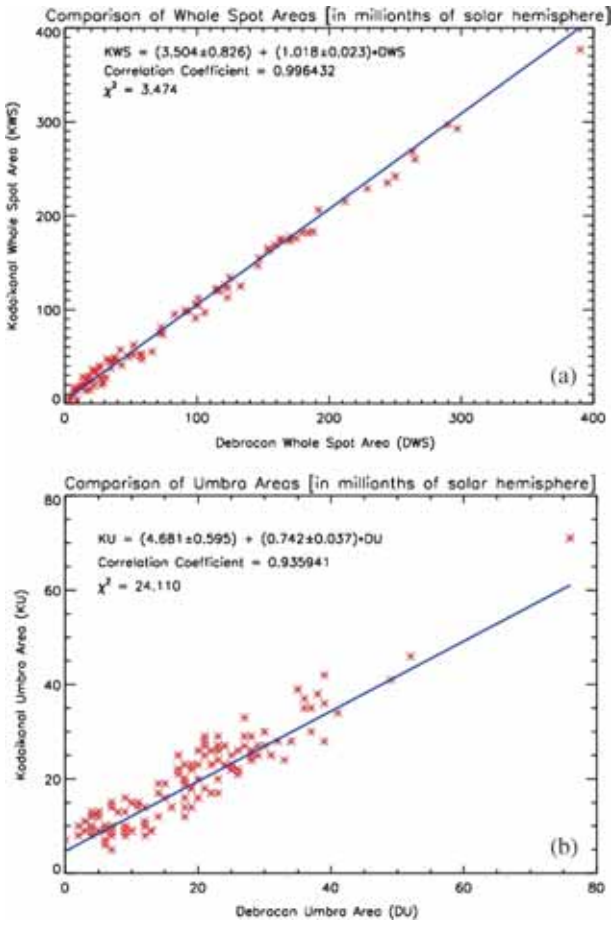

Figure 8. A scatter plot of Kodaikanal and Debracen data for area of sunspots. (**a**) The scatter plot for whole spot area, and (**b**) the scatter plot for umbral area of the sunspots.

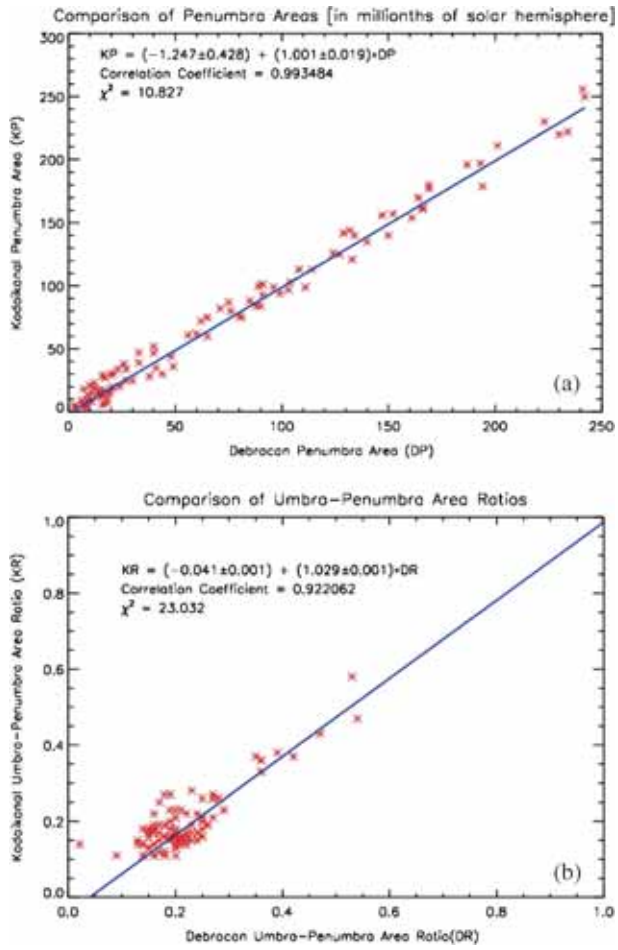

Figure 9. A scatter plot of Kodaikanal and Debracen data for area of sunspots. (**a**) The scatter plot for penumbral area of sunspots and (**b**) the scatter plot for umbra–penumbra area ratio of sunspots.

computation of χ^2. However, as the estimated errors are very small ($\sim$1%) and χ^2 is inversely proportional to estimated errors, apparent value of χ^2 is very large. In order to avoid this inconsistency, all the parameters with their error bars are normalized and χ^2 is computed. From all the illustrated plots, one can notice that χ^2 is very small suggesting good association between both the results.

From the monthly variation of whole spot area and umbra–penumbra area ratio plots, it is clear that both the Kodaikanal and Debracen results follow a similar trend and moreover, the Debracen results are well within the error bars.

4.1 *Advantages and disadvantages of the new method*

For all the algorithms described in section 3, an IDL code is developed to detect sunspots and to estimate their parameters from the digitized images of the Kodaikanal

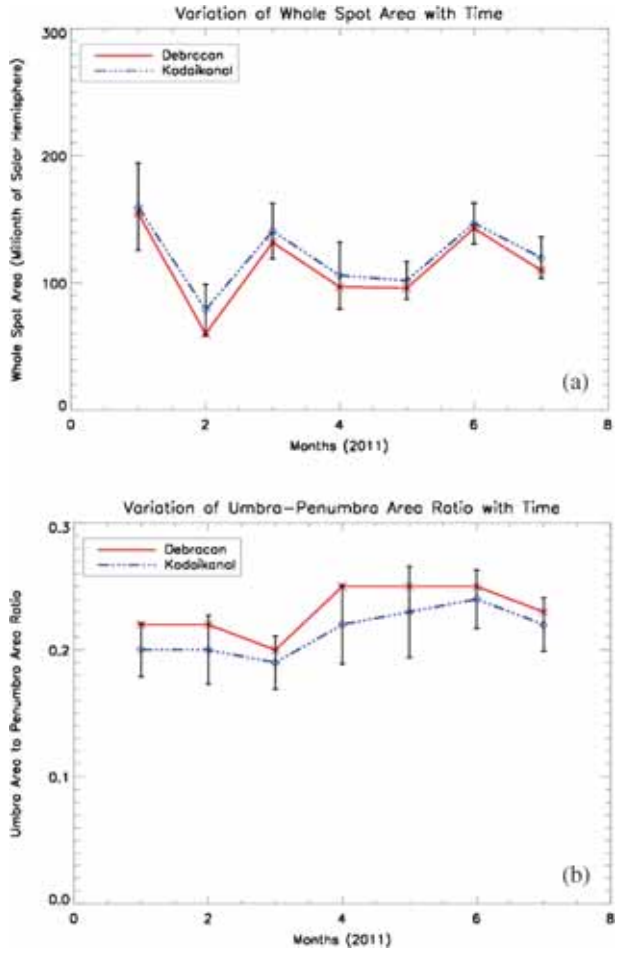

Figure 10. Monthly variation of whole spot area and umbra–penumbra area ratio of Kodaikanal and Debracen sunspot data. (**a**) The variation of whole spot area and (**b**) the variation of umbra–penumbra area ratio.

Observatory. This code automatically detects the edge of the solar disc, computes its radius and center simultaneously and uniquely, removes limb-darkening and computes heliographic coordinates – all in one go. It also automatically detects the sunspots and estimates the required parameters, whose results perfectly match with those of the already existing results, such as the Debracen sunspot results. Our method also computes the error bars in all the estimates, making the computation more accurate. This IDL code is fully-automatic, thus reducing the errors introduced by human bias.

However, an important disadvantage of this code is that our method uses a certain intensity threshold for umbra detection, which is not particularly unique. One more disadvantage lies with the thin wire across each image, that produces some unwanted results in few of the images.

5. Conclusion

A fully automized algorithm was successfully developed to analyze the Kodaikanal solar white light images. The algorithm includes computation of the radius and center of the solar disc simultaneously and uniquely. Our developed algorithm further detects sunspots and estimates the average latitude and longitude from central meridian of each of the detected sunspots. It separates the umbra from each sunspot and computes the area of both the whole spot and the umbra. The results obtained are compared with the existing Debracen data and it is found that the heliographic coordinates of sunspots and their areas, estimated by our method are almost similar to the Debracen results. Hence, this validates our methodology of detection of sunspots and estimation of area and their respective heliographic coordinates.

Acknowledgements

The authors are thankful to the referee for useful comments and suggestions. The first author is grateful to the Director, Dr. P. Sreekumar, the Dean and BGS for providing financial support, accommodation and allowing to use the library and computer facilities during her visit to Indian Institute of Astrophysics. The first author is also thankful to Dr. Ravindra and Suryanarayana for useful discussions. The authors thankfully acknowledge all the digitization team of the Kodaikanal Observatory Solar images.

Appendices

Appendix A

Circle-fitting

Let x_i and y_i be the x- and y-coordinates of the edge detected pixels (as illustrated in Figure 2), respectively, where i varies from 1 to N, given N is the total number of detected pixels. Let $\bar{x}$ and $\bar{y}$ be the mean of the respective x_i and y_i coordinates. That is,

$$\bar{x} = \frac{\Sigma x_i}{N}$$

and

$$\bar{y} = \frac{\Sigma y_i}{N}.$$

Firstly, we convert the (x_i, y_i) coordinates into a new system of coordinates (u_i, v_i) with

$$u_i = x_i - \bar{x}$$

and

$$v_i = y_i - \bar{y}.$$

Let (u_c, v_c) be the center of the circle and let R be its radius in this new coordinate system. Let $\alpha = R^2$.

Distance of any point (u_i, v_i) from the center is $= \sqrt{(u_i - u_c)^2 + (v_i - v_c)^2}$.

According to the least square fit, best fit is obtained when the function $S = \sum_i [g(u_i, v_i)]^2$ is minimized, where $g(u_i, v_i) = (u_i - u_c)^2 + (v_i - v_c)^2 - \alpha$. Hence, the partial derivatives of these functions with respect to α, u_c and v_c should all be zero.

Condition 1:

$$\frac{\partial S}{\partial \alpha} = 2 \times \sum_i g[u_i, v_i] \frac{\partial g}{\partial \alpha} = 0 \tag{A1}$$

$$\Rightarrow -2 \times \sum_i g[u_i, v_i] = 0$$

$$\Rightarrow \sum_i [(u_i - u_c)^2 + (v_i - v_c)^2 - \alpha] = 0$$

$$\Rightarrow \sum_i {u_i}^2 + \sum_i {u_c}^2 + \sum_i {v_i}^2 + \sum_i {v_c}^2 - 2\left[\sum_i u_i u_c + \sum_i v_i v_c\right] = \sum_i \alpha$$

$$\Rightarrow \sum_i {u_i}^2 + \sum_i {v_i}^2 + N[{u_c}^2 + {v_c}^2] - 2\left[u_c \sum_i u_i + v_c \sum_i v_i\right] = N\alpha\,. \tag{A2}$$

It is known that $\sum_i u_i = \sum_i (x_i - \bar{x}) = N\bar{x} - N\bar{x} = 0$. Similarly, $\sum_i v_i = 0$. Putting this in equation (A2), we get

$$\sum_i {u_i}^2 + \sum_i {v_i}^2 + N[{u_c}^2 + {v_c}^2] = N\alpha\,. \tag{A3}$$

Condition 2:

$$\frac{\partial S}{\partial u_c} = 2 \times \sum_i g[u_i, v_i] \frac{\partial g}{\partial u_c} = 0,$$

$$\Rightarrow \sum_i (u_i - u_c) g(u_i, v_i) = 0. \tag{A4}$$

On expansion,

$$\Rightarrow \sum_i {u_i}^3 + \sum_i u_i {v_i}^2 - 2u_c \sum_i {u_i}^2 - 2v_c \sum_i u_i v_i - u_c \sum_i {u_i}^2 - u_c \sum_i {v_i}^2 - N{u_c}^3 - N u_c {v_c}^2 + N\alpha u_c = 0.$$

Substituting the value of $N\alpha$ from equation (A3), the following equation is obtained:

$$u_c \sum_i {u_i}^2 + v_c \sum_i u_i v_i = \frac{1}{2}\left[\sum_i {u_i}^3 + \sum_i u_i {v_i}^2\right]. \tag{A5}$$

Condition 3:

$$\frac{\partial S}{\partial v_c} = 2 \times \sum_i g[u_i, v_i] \frac{\partial g}{\partial v_c} = 0\,. \tag{A6}$$

Proceeding the same way as in Condition 2, the following equation is obtained:

$$u_c \sum_i u_i v_i + v_c \sum_i {v_i}^2 + = \frac{1}{2}\left[\sum_i {v_i}^3 + \sum_i v_i {u_i}^2\right]. \tag{A7}$$

Solving simultaneous equations (A5) and (A7), the values of u_c and v_c are obtained. Then from equation (A3),

$$\alpha = R^2 = ({u_c}^2 + {v_c}^2) + \frac{1}{N}\left[\sum_i {u_i}^2 + \sum_i {v_i}^2\right], \tag{A8}$$

and

$$R = \sqrt{\alpha} = \sqrt{({u_c}^2 + {v_c}^2) + \frac{1}{N}[\Sigma {u_i}^2 + \Sigma {v_i}^2]}\,. \tag{A9}$$

From this equation, the value of radius, R of the solar disc is estimated. The next step is, converting (u_c, v_c) into the original coordinate system, that is obtained by adding the respective mean values

$$x_c = u_c + \bar{x}$$

and

$$y_c = v_c + \bar{y}.$$

Hence, using this method, the coordinates of the center of the image (x_c, y_c) and the radius R, is computed uniquely.

Appendix B

Heliographic coordinates

Following Smith (1990), we compute the heliographic coordinates of the sunspots as follows. To compute the heliographic latitude θ, heliographic longitude L and longitude difference from central meridian l, it is necessary to calculate the daily values of heliographic latitude (B_o) and longitude (B_o) of the disk center as well as the polar angle P.

Let $T = \frac{\text{JD}-2415020}{36525}$, where JD is the Julian Date of observation and T is the number of Julian centuries since epoch 1900 Jan 0.5.

The geometric mean latitude L', mean anomaly g and right ascension Ω of the ascending node of the Sun are

$$L' = 279^\circ.69668 + 36000^\circ.76892T + 0^\circ.0003025T^2,$$
$$g = 358^\circ.47583 + 35999^\circ.04975T - 0^\circ.00015T^2 - 0^\circ.0000033T^2$$

and

$$\Omega = 259^\circ.18 - 1934^\circ.142T.$$

The true longitude $\lambda_\odot$, of the Sun is given by

$$\lambda_\odot = L' + C,$$

where C is called the equation of the center and is defined as

$$\begin{aligned} C &= (1^\circ.91946 - 0^\circ.004789T - 0^\circ.000014T^2)\sin(g) \\ &\quad +(0^\circ.020094 - 0^\circ.0001T)\sin(2g) + 0^\circ.000293\sin(3g). \end{aligned}$$

The apparent longitude of the Sun, λ_a consists of the true longitude, $\lambda_\odot$ and corrections for aberration and nutation

$$\lambda_a = \lambda_\odot - 0^\circ.00569 - 0^\circ.00479\sin(\Omega).$$

The actual physical ephemeris computations begin with

$$\phi = \frac{360}{25.38}(\mathrm{JD} - 2398220).$$

The inclination of the equator of the Sun relative to the ecliptic plane is $I = 7.25^\circ$ and the longitude of the ascending node of the solar equator, K is

$$K = 74^\circ.3646 + 1^\circ.395833T.$$

X and Y are defined such that

$$\tan(X) = -\cos(\lambda')\tan(\epsilon)$$

and

$$\tan(Y) = -\cos(\lambda_\odot - K)\tan(I),$$

where ϵ is the obliquity of the ecliptic and λ' is the Sun's apparent longitude corrected for nutation.

The mean obliquity ϵ_o is determined from

$$\epsilon_\mathrm{o} = 23^\circ.452295 - 0^\circ.0130125T - 0^\circ.00000164T^2 + 0^\circ.0000005503T^3,$$

and with the correction of nutation as

$$\epsilon = \epsilon_\mathrm{o} + 0^\circ.00256\cos(\Omega).$$

Finally, polar angle P, B_o and L_o can be computed as follows:

$$\begin{aligned} P &= X + Y, \\ B_\mathrm{o} &= \sin^{-1}[\sin(\lambda_\odot - K)\sin(I)], \\ L_\mathrm{o} &= \tan^{-1}\left[\frac{\sin(K - \lambda_\odot)\cos(I)}{-\cos(K - \lambda_\odot)}\right] + M, \end{aligned}$$

where $M = 360^\circ - \phi$. ϕ must be reduced to the range $0^\circ - 360^\circ$ by subtracting integral multiples of 360°.

The solar radius as viewed from the Earth changes daily due to the revolution of Earth around the Sun. Hence, the resolution of the pixels changes daily as well.

If n is the number of days from J2000.0, the mean anomaly g, measured from the epoch J2000.0 is defined as follows:

$$n = \text{JD} - 2451545.0,$$
$$g = 357^\circ.528 + 0^\circ.9856003\, n.$$

g is reduced to the of range 0° to 360° by adding multiples of 360°. Distance of the Sun from Earth, R', in AU is

$$R' = 1.00014 - 0.01671\cos(g) - 0.00014\cos(2g).$$

The semi-diameter of the Sun, Rad in arc-seconds is

$$\text{Rad} = \left(\frac{0.2666}{R'}\right)^\circ \times 3600''.$$

Mathematical determination of the heliographic coordinates is based on the polar coordinates (r, θ'). This means, before computation of heliographic coordinates, the observed Sun's image in cartesian coordinates is transformed to polar coordinates. The angular distance ρ of any pixel from the center of the solar disc is then determined from the equation

$$\sin(\rho) = \frac{r}{R},$$

where R is the radius of the solar disc as described in Appendix A, using circle fit. To calculate the heliographic latitude θ and longitude l from the central meridian of any pixel, the following equations are used:

$$\sin(\theta) = \cos(\rho)\sin(B_\text{o}) + \sin(\rho)\cos(B_\text{o})\sin(\theta'),$$
$$\sin(l) = \frac{\cos(\theta')\sin(\rho)}{\cos(\theta)}.$$

The heliographic longitude is obtained by adding the value of L_o to the the longitudinal difference l of the pixel from the central meridian.

$$L = L_\text{o} + l.$$

For more accurate results, correction for distortion of the Sun's image is considered. Telescope objective lens with a short focal length can contribute to distortion of the projected image. This distortion is corrected by using the following empirical relations:

$$T = \frac{\text{Rad}}{15},$$
$$R_\text{o} = 29.5953\,\cos\left[\frac{\cos^{-1}(-0.00629T)}{3} + 240\right],$$
$$\rho' = R_\text{o} \times \frac{r}{R}$$

and

$$\rho = \sin^{-1}\left(\frac{\sin(\rho')}{\sin(R_\text{o})}\right) - \rho'.$$

This ρ is then taken as the corrected angular distance and then the heliographic coordinates are computed as mentioned above.

References

Baranyi, T., Ludmany, A. 1992, *Solar Phys.*, **139**, 247.
Baranyi, T., Ludmany, A., Groyi, L. *et al.* 1999, *ESA-SP*, 448.
Cakmak, H. 2014, *Experimental Astron.*, **37**, 539.
Chapman, G. A., Walton, S. R. 2001, American Geophysical Union, Spring Meeting.
Csilla, Szasz 2003, Ph.D. Thesis.
Curto, J. J., Blanca, M., Martinez, E. 2008, *Solar Phys.*, **250**, 411.
Denker, C., Johannesson, A. *et al.* 1998, *Solar Phys.*, **184**, 87.
Goel, S., Mathew, S. K. 2014, *Solar Phys.*, **289**, 1413.
Grossmann-Doerth, U., Schmidt, W. 1981, *A&A*, **95**, 366.
Gyori, L. 1998, *Solar Phys.*, **180**, 109.
Hiremath, K. M. 2006a, Proc. ILWS Workshop, edited by Gopalswamy, N. & Bhattacharyya, A., p. 178.
Hiremath, K. M. 2006b, *Journal of Astron. Astrophys.*, **27**, 367.
Hiremath, K. M. 2009, *SunGe*, **4(1)**, 16.
Hiremath, K. M., Hegde, M. 2013, *ApJ*, **763**, 137.
Hiremath, K. M., Hegde, M., Soon, W. 2015, *New Astron.*, **35**, 8.
Hiremath, K. M., Lovely, M. R. 2010, preprint(2010arXiv1012.5706H).
Hiremath, K. M., Mandi, P. I. 2004, *New Astron.*, **9(8)**, 651.
Howard, R. F. 1991, *Solar Phys.*, **136**, 251.
Howard, R. F. 1992, *Solar Phys.*, **142**, 233.
Howard, R., Gilman, P. A., Gilman, P. I. 1984, *ApJ*, **283**, 373.
Lustig, G., Wohl, H. 1995, *Solar Phys.*, **137**, 389.
Oliver, R., Ballester, J. L. 1995, *Solar Phys.*, **165**, 145.
Pettauer, T., Brandt, P. N. 1997, *Solar Phys.*, **175**, 197.
Poljancic, I., Brajsa, R., Hrzina, D. *et al.* 2011, *Cent. Eur. Astrophyc. Bull.*, **35(1)**, 59.
Ravindra, B., Priya, T. G. *et al.* 2013, *A&A*, **500**, A19.
Singh, J., Ravindra, B. 2012, *Bull. Astr. Soc. India*, **40**, 77.
Sivaraman, K. R., Gupta, S. S. 1993, *Solar Phys.*, **146**, 27.
Smith, P. D. 1990, in: *Practical Astronomy with your calculator*, Cambridge University Press.
Steinegger, M., Brandt, P. N., Schimidt, W. 1990, *Astonomicscche Gesellschaft Abstract Series*, **5**, 42.
van Driel-Gesztelyi, Csepura, G., Nagy, I. *et al.* 1993, *Solar Phys.*, **145**, 77.
Watson, F., Fletcher, L., Dalla, S. *et al.* 2009, *Solar Phys.*, **260**, 5.
Yu, L., Deng, L., Song, F. 2014, *Proc. 33rd Chinese Control Conference*, July 28–30.
Zharkov, S., Zharkov, V., Ipson, S. *et al.* 2005, *EURASIP Journal in Applied Signal Processing*, **15**, 2573.